Iris Pupil Detection by Structure Tensor Analysis

Fernando Alonso-Fernandez and Josef Bigun
Halmstad University. Box 823. SE 301-18 Halmstad, Sweden
{Fernando.Alonso-Fernandez,Josef.Bigun}@hh.se

***Abstract*—This paper present a pupil detection/segmentation algorithm for iris images based on Structure Tensor analysis. Eigenvalues of the structure tensor matrix have been observed to be high in pupil boundaries and specular reflections of iris images. We exploit this fact to detect the specular reflections region and the boundary of the pupil in a sequential manner. Experimental results are given using the CASIA-IrisV3-Interval database (249 contributors, 396 different eyes, 2,639 iris images). Results show that our algorithm works specially well in detecting the specular reflections (98.98% success rate) and pupil boundary detection is correctly done in 84.24% of the images.**

I. Introduction

Biometric authentication has been receiving considerable attention over the last years due to the increasing demand for automatic person recognition. The term "biometrics" refers here to automatic recognition of an individual based on behavioral and/or physiological characteristics (e.g., fingerprints, face, iris, voice, signature, etc.), which cannot be stolen, lost, or copied [1]. Among all biometric techniques, iris recognition has been traditionally regarded as one of the most reliable and accurate biometric identification system available [2].

The iris is a colored ring of tissue around the pupil through which light enters the interior of the eye. Figure 1 shows an example image of a captured iris. The sclera is the white region that surrounds the outer part of the iris. The pupil region generally appears darker than the iris and may also have specular reflections as a result of light sources typically used in commercial acquisition systems. The details of the iris texture are believed to be different between different people and also between the left and right eye of the same person, thus providing a valuable source for personal recognition [3].

Iris analysis begins with the detection of the inner and outer boundaries of the iris. The success of this task is crucial for the good performance of a iris recognition system. Early works include the Daugman's approach using an integro-differential operator [4] and the method of Wildes involving edge detection and circular Hough transform [5]. They are based on the assumption that the boundaries of the iris can be modeled as two concentric circles. Much of the subsequent research in this area has tried to improve the Wildes idea of using edge detection and a Hough transform, with suggestions to improve its inherent computational burden or the lack of enough edge points to define a circle [2].

In this paper, we come up with a pupil detection/segmentation algorithm for iris images based on analysis of the Structure Tensor. In a sequential fashion, we first detect the specular reflections that typically appear within the pupil and then, we detect the pupil region. In the proposed method, no assumption is made about circularity of the pupil, thus allowing the detection of non-circular or irregular pupil boundaries. Reported results show the effectiveness of the proposed algorithm with good quality images. One drawback of the algorithm is the assumption that the pupil boundary is a closed curve. Relaxing this assumption would allow the correct detection in worse conditions, namely in the presence of eyelashes/eyelids occlusion, spurious reflections, off-angle images, etc [6].

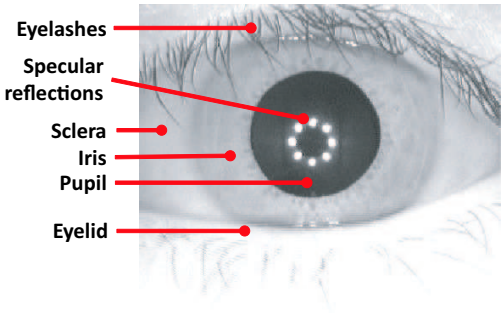

Fig. 1. Iris image with typical elements labeled.

II. The 2D Structure Tensor

Given a gaussian smoothed image $I[p]$, where $p = [x, y]$ is the coordinates of a point in 2D, the 2D Structure Tensor $S_w[p]$ at a given pixel p is the 2×2 matrix [7]:

$$S_w[p] = \sum_r w[r] \begin{bmatrix} (I_x[p])^2 & I_x[p] I_y[p] \\ I_x[p] I_y[p] & (I_y[p])^2 \end{bmatrix} \quad (1)$$

with the summation index r ranging over a set of coordinate pairs $\{-m...m\} \times \{-m...m\}$ and $w[p]$ a weighting window centered at p (typically gaussian) such that the sum of all weights is 1. The values $I_x[p]$ and $I_y[p]$ are the estimated partial derivatives of image $I[p]$ at pixel p.

If we rewrite the matrix of Eq. 1 as

$$S_w[p] = \begin{bmatrix} a & c \\ c & b \end{bmatrix} \quad (2)$$

then the eigenvalues λ_1, λ_2 of $S_w[p]$ (ordered so that $\lambda_1 \geq \lambda_2$) are found to be:

$$\lambda_1 = 0.5 * (a + b + \sqrt{(a-b)^2 + 4c^2}) \quad (3)$$

$$\lambda_2 = 0.5 * (a + b - \sqrt{(a-b)^2 + 4c^2}) \quad (4)$$

The importance of the 2D Structure Tensor $S_w[p]$ is given by the fact that the eigenvalues λ_1, λ_2 (and their corresponding eigenvectors e_1, e_2) summarize the distribution of the gradient $\nabla I = (I_x, I_y)$ of image $I[p]$ within the window $w[p]$. If for example $\lambda_1 > \lambda_2$, then eigenvector e_1 gives the direction that is maximally aligned with the gradient within $w[p]$. In particular, if $\lambda_1 > 0$ $\lambda_2 = 0$ then the values of $I[p]$ within the window varies along the direction e_1 and are constant along e_2. On the other hand, if $\lambda_1 = \lambda_2$, the gradient in $w[p]$ has no predominant direction (balanced directions), which is the case for instance when there is rotational symmetry within that window. In particular, if $\lambda_1 = \lambda_2 = 0$, then $I[p]$ is constant within $w[p]$ ($\nabla I = (I_x, I_y) = (0, 0)$).

III. Iris Pupil Detection by Structure Tensor Analysis

We propose the use of the Structure Tensor to detect and segment the pupil region of iris images. In Figure 2, we depict eigenvalues λ_1 and λ_2 of the iris image shown in Figure 1 for different sizes of the weighting gaussian window $w[p]$. Iris image is pre-smoothed using a gaussian window of size 3×3 and standard deviation $\sigma = 1.5$. The overall model of our detection/segmentation system is depicted in Figure 3, which is described next.

It can be observed in Figure 2 that eigenvalue λ_2 exhibits their highest values in the specular reflections, specially when the window $w[p]$ is of enough size to detect the rotational symmetry around the center of the reflection point (recall that higher λ_2 means more anisotropy of the gradient). For a window $w[p]$ of size 20×20, we first detect the maximum of λ_2. We then binarize the image of λ_2 by using the Otsu method [8] and select the connected binary element which falls on the detected maximum. The border of the selected binary element will give us the boundaries of the specular reflections region. Also, the centroid of the binary element will be the centroid of the specular reflections. The whole process can be seen in Figure 3, top.

After detecting the border and centroid of the specular reflections region, we use λ_1 as follows to find the boundary of the pupil. It can be observed in Figure 2 that λ_1 exhibits their highest values in the boundaries of the pupil region and the specular reflections, as well as on the eyelashes region. Increasing the size of the weighting window $w[p]$ has an averaging effect, resulting in lower spatial resolution and more diffused boundaries. We first binarize with the Otsu method [8] the image of λ_1 obtained with a window $w[p]$ of size 3×3. Then, we remove from the binarized image the region of the specular reflections previously detected and finally, we apply the watershed transform [9]. When doing so, the connected element which falls on the centroid of the specular reflections region should correspond with the iris pupil. This process can be seen in Figure 3, bottom. We impose the condition that the size of the detected pupil should not exceed a percentage of the total image size (50% in our experiments), otherwise the image is marked as "non passing" the segmentation stage.

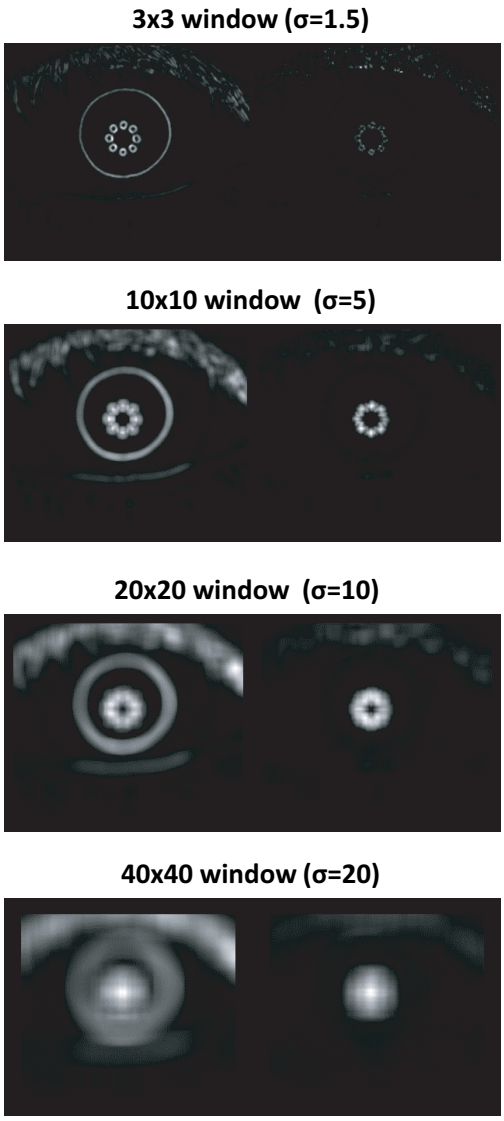

Fig. 2. Eigenvalues λ_1 (left column) and λ_2 (right column) of the iris image of Figure 1 for different sizes of the weighting gaussian window $w[p]$. To depict the eigenvalues, they are re-scaled so that white represents the maximum eigenvalue of the image and black represents 0 by using 256 gray tones and linear mapping.

For a given size of the pupil, one can also detect the pupil by means the Generalized Structure Tensor (GST), [10], which is essentially template matching in the tensor domain, and can be conveniently expressed using complex version of the structure tensor i.e.

$$I_{20} = \sum_p c(p)(I_x(p) + iI_y(p))^2 \qquad (5)$$

where $c(p)$ is defined as the complex version of the structure tensor response of a circle:

$$c(p) = \exp(-i2\varphi)(x^2 + y^2)^\gamma \exp(-\frac{x^2 + y^2}{2\sigma_2^2}) \qquad (6)$$

Here γ and σ_2 are parameters that together determine the radius of the pupil and the precision of the filter (width of the pupil boundary region). It can be shown that, a high response in terms of the magnitude of I_{20} and zero argument of I_{20} is obtained at a point, if there are edges

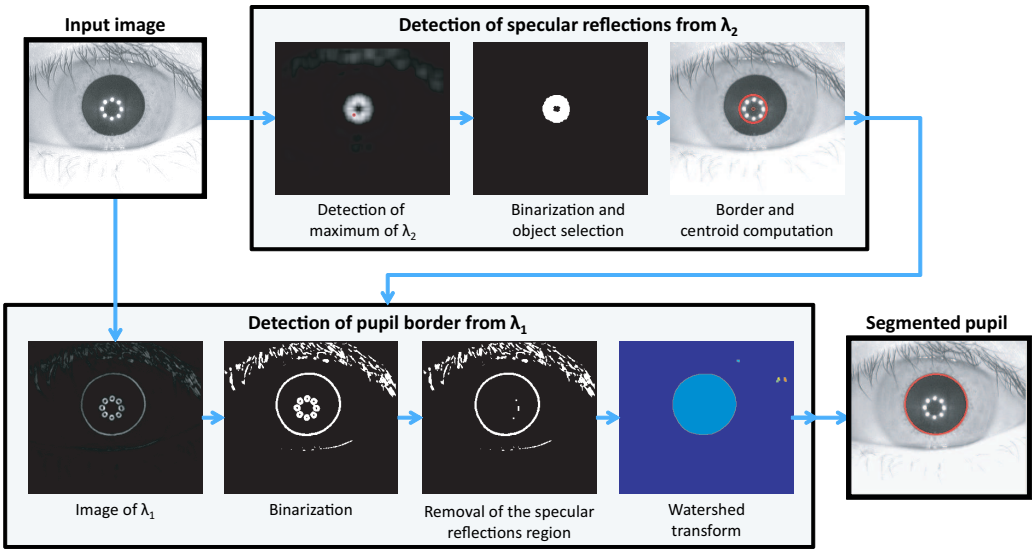

Fig. 3. System model for pupil detection/segmentation by Structure Tensor analysis.

Results (total images: 2259)
Correct detection of specular reflection: 2236 (98.98%)
Images passing the segmentation stage: 1946 (86.14%)
Images correctly segmented: 1903 (84.24%)

TABLE I
RESULTS OF THE DIFFERENT STAGES OF OUR PUPIL DETECTION/SEGMENTATION ALGORITHM.

at the prescribed (same) distance from that point and there is an agreement in terms of local orientations (structure tensors) with those of a circle. The GHT based detection can be selectively applied to the candidate centers to verify the found pupil to avoid false acceptance.

IV. Database and Protocol

We have used for the experiments the "Interval" set of the CASIA-IrisV3 database [11], captured at the Chinese Academy of Sciences' Institute of Automation (CASIA). Iris images of this dataset were acquired with a close-up iris camera that includes a circular NIR LED array. This array produces a circular set of specular reflection points as can be seen in Figure 1. CASIA-IrisV3-Interval includes 2,639 iris images of 280 pixels height and 320 pixels width from 249 contributors acquired in two sessions. The number of images per contributor and per session is not constant and not all the individuals have images of the two eyes. The number of different eyes included in the database is 396.

The experimental protocol is as follows. The training set comprises two iris images from each individual (one from each eye, if available), resulting in 396 images. Images from the training set are used to infer the parameters of Section III after running the detection/segmentation algorithm for a comprehensive combination of the different parameters involved. The remaining 2,639-396=2,259 iris images are used as test set to compute success rates of our algorithm given in Section V. No training or inference of parameters is done on the test set.

V. Experimental Results

In Table I, we give the success rates of the different stages of our detection/segmentation algorithm on the test set. Except for the number of images passing the segmentation stage (which is computed automatically), the other two figures are manually obtained after reviewing the resulting segmented images.

Correct detection of specular reflections is done in 98.98% of the images (Figure 4 depicts some examples of correct and non-correct images). When the detection is not made correctly, it is mainly due to eyelids occlusion, secondary specular reflections and/or lack of one of the reflection spots (probably due to a blown lamp). Although the shape of the detected region is not as expected, however, estimation of the centroid is not very affected.

According to Table I, 1946 images (86.14%) pass the segmentation stage, meaning that a connected element is detected by the watershed transform and it complies with the size condition imposed (see Section III). However, after manual review, it turns out that the iris region is well detected in 1903 images (84.24%). Some examples are shown in Figure 5a. In the remaining 1946-1903=43 images, the boundary of the pupil is not well detected, mainly due to eyelids/eyelashes occlusion or to secondary specular reflections. Some examples of these issues are shown in Figure 5b. Finally, there are 2259-1946=313 images that do not pass the segmentation stage (some examples are depicted in Figure 5c). In all cases, it is because the pupil boundary in λ_1 is not a closed curve, so the watershed algorithm is not able to detect it. Reasons for an open curve, as can be seen Figure 5c, are the occlusion of eyelashes or the presence of primary/secondary specular reflections in the boundary of the pupil.

VI. Conclusion

A pupil detection/segmentation algorithm for iris images by Structure Tensor analysis has been proposed. It is based in the observations that pupil boundaries

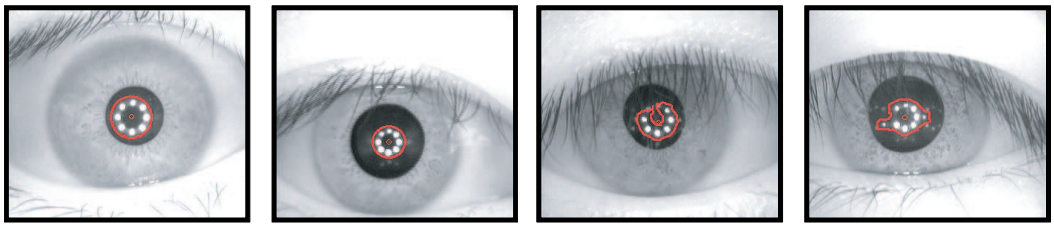

(a) Correct detection of specular reflections (b) Non-correct detection of specular reflections

Fig. 4. Examples of images with correct detection of specular reflections (a) and non-correct detection (b).

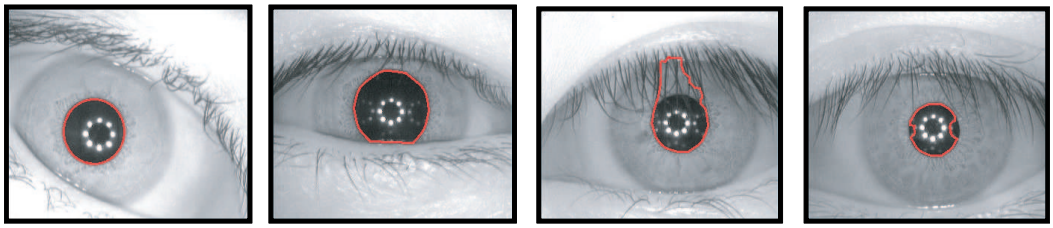

(a) Correct pupil detection (b) Incorrect pupil detection

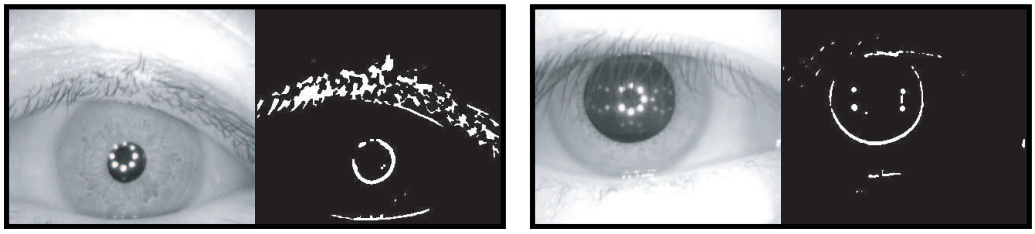

(c) Pupil detection error (left part: iris image, right part: binarized λ_1 with the region of the specular reflections removed)

Fig. 5. Examples of images with correct pupil segmentation (a), incorrect pupil segmentation (b) and errors in the segmentation (c).

and specular reflections of the image are regions with high value of eigenvalues λ_1 and λ_2, respectively. Also, specular reflections typically appear in iris images within the pupil boundary. These facts are exploited to firstly detect the specular reflections region and then, to find the boundary of the pupil.

Experimental results show that our algorithm works specially well in detecting the specular reflections from λ_2. Although the specular reflections of the database used here have a particular distribution as a circular array of points, the above observation remains valid for any given distribution, because reflection points are usually the brightest points in iris images. Since the number and distribution of reflection points is typically known for a given acquisition sensor, the proposed algorithm could be adapted accordingly.

Concerning the detection of the iris boundary, it is well detected in 84.24% of the test images. Incorrect functioning of the algorithm mainly occurs due to eyelashes occluding part of the pupil boundary or due to spurious specular reflections appearing in different regions of the pupil. Our algorithm relies in the fact that the pupil boundary appears in λ_1 as a closed curve, which is not always true in the presence of the mentioned factors. In this sense, our algorithm would benefit of other complementary alternatives such as the traditional hough transform or active shape models [2] when the circular curve that surrounds the pupil is not closed. This capability is essential in images acquired in less-controlled conditions, and it will be the source of future work.

ACKNOWLEDGMENT

Author F. A.-F. thanks the Swedish Research Council (Vetenskapsrådet) for its financial support. Portions of this research use the CASIA-IrisV3 collected by the Chinese Academy of Sciences' Institute of Automation (CASIA).

REFERENCES

[1] A. Jain, A. Ross, and S. Prabhakar, "An introduction to biometric recognition," *IEEE Trans. CSVT*, vol. 14, no. 1, pp. 4–20, 2004.
[2] K.W. Bowyer, K. Hollingsworth, and P. Flynn, "Image understanding for iris biometrics: a survey," *Computer Vision and Image Understanding*, vol. 110, pp. 281–307, 2007.
[3] E. Newton and P. Phillips, "Meta-analysis of third party evalutions of iris recognition," *NISTIR 7440*, 2007.
[4] J. Daugman, "How iris recognition works," *IEEE Trans. CSVT*, vol. 14, pp. 21–30, 2004.
[5] R. P. Wildes, "Iris recognition: An emerging biometric technology," *Proc. IEEE*, vol. 85, no. 9, pp. 1348–1363, 1997.
[6] J. Matey, O. Naroditsky, K. Hanna, R. Kolczynski, D. LoIacono, S. Mangru, M. Tinker, T. Zappia, and W. Zhao, "Iris on the move: acquisition of images for iris recognition in less constrained environments," *Proc. IEEE*, vol. 94, no. 11, pp. 1936–1946, 2006.
[7] J. Bigun, G. Granlund, "Optimal orientation detection of linear symmetry," *Intl Conf Computer Vision, ICCV*, pp. 433–438, 1987.
[8] N. Otsu, "A threshold selection method for gray-level histograms," *IEEE Trans. SMC*, vol. 9, pp. 62–66, 1979.
[9] F. Meyer, "Topographic Distance and Watershed Lines," *Signal Processing*, vol. 38, pp. 113–125, 1994.
[10] J. Bigun, *Vision with Direction.* Springer, 2006.
[11] CASIA Iris Image Database, "http://biometrics.idealtest.org."